International Symposium
On Turbulence and Shear Flow
Phenomena (TSFP-9)
June 30 - July 3, 2015 *Melbourne, Australia*

NUMERICAL STUDIES OF ACTIVE CONTROL OF TURBULENT BOUNDARY LAYERS USING TRANSVERSE TRAVELLING WAVES

Martin Skote
School of Mechanical and Aerospace Engineering
Nanyang Technological University
50 Nanyang Avenue, Singapore 639798, Singapore
mskote@ntu.edu.sg

Philipp Schlatter
Linné FLOW Centre
KTH Mechanics
Stockholm, Sweden
pschlatt@mech.kth.se

Yanhua Wu
School of Mechanical and Aerospace Engineering
Nanyang Technological University
50 Nanyang Avenue, Singapore 639798, Singapore
YanhuaWu@ntu.edu.sg

ABSTRACT

Turbulence control in the form of transverse wall motion is employed numerically (direct numerical simulation). Results from a turbulent boundary layer subjected to spanwise wall forcing in the form of a streamwise travelling wave are presented for the first time.

Both total and phase averaging have been utilized to examine the statistical behaviour of the turbulence affected by the wall forcing. Various statistical quantities are examined and compared with results from pure temporal and spatial wall forcing. Furthermore, interesting analogies with the channel flow are discussed.

INTRODUCTION

The first observations of wall oscillation as means for DR was made by Jung *et al.* (1992) through direct numerical simulations (DNS) of a channel flow. Since then, a lot of research efforts have been made in this direction for internal flow such in a channel or pipe flow. The boundary layer flows have only recently started to be investigated numerically (Yudhistira & Skote (2011); Skote (2011, 2012, 2013, 2014); Lardeau & Leschziner (2013)), while experiments have previously been performed by quite a number of researchers. In fact, the first experimental evidence that confirmed that Jung's DNS results was provided by Laadhari *et al.* (1994) and Skandaji (1997), who applied the oscillation technique to the boundary layer flow. Since then, most of the experimental investigations have been focused on the boundary layer (Trujillo *et al.*, 1997; Choi & Clayton, 2001; Choi, 2002; Di Cicca *et al.*, 2002; Ricco, 2004; Ricco & Wu, 2004). Extensive comparison between DNS, using the same numerical code as in the present work, and these experiments were made by Yudhistira & Skote (2011)

The most commonly form of control studied is realized with a temporal wall oscillations, which is imposed through a wall velocity (W) in the spanwise direction in the form of

$$W = W_m \sin(\omega t), \tag{1}$$

where W_m is the maximum wall velocity and ω is the angular frequency of the wall oscillation, which is related to the period (T) through $\omega = 2\pi/T$.

The oscillation in time is relatively straightforward to implement in an experimental setting, however, a positive energy budget may not be easily obtained. Instead, researchers (Viotti *et al.*, 2009; Skote, 2011, 2013; Negi *et al.*, 2015) have considered a steady variation in the streamwise direction along the plate instead of a time-dependent forcing. In this case, the wall velocity (W) is imposed in the form of

$$W = W_m \sin(\kappa x), \tag{2}$$

where κ is the wavenumber of the spatial oscillation, which is related to the wavelength (λ_x) through $\kappa = 2\pi/\lambda_x$.

Quadrio *et al.* (2009) have studied (through DNS) the combination of spatial and temporal wall oscillation (stream-wise travelling waves) in a channel flow. The theoretical and numerical studies were further developed by Quadrio & Ricco (2011). The travelling waves as wall forcing were implemented in the form of

$$w(x,t) = W_m \sin(\kappa x - \omega t) \tag{3}$$

by Quadrio *et al.* (2009). A diverse behaviour, showing regions of both DR and drag increase (DI) in the wavenumber-angular frequency space, was discovered when varying the parameters.

The only experimental data to date for this type of wall forcing are provided by Auteri *et al.* (2010), who applied the streamwise travelling wave on the pipe flow. To our knowledge, the current work constitutes the first attempt to study wall forcing by travelling waves in the boundary layer.

METHODOLOGY

The numerical code and grid are the same as in the previous simulations of a spatially oscillating turbulent bound-

ary layer reported by Skote (2011). The code was developed at KTH, Stockholm (Chevalier *et al.*, 2007). A simulation of a turbulent boundary layer at $Re_\Theta = 2500$ was performed by Schlatter *et al.* (2009) with results in excellent agreement with experimental data at the same Reynolds number.

Numerical scheme

A pseudo-spectral method is employed, with Fourier discretization used in the streamwise and spanwise directions, and Chebyshev polynomials in the wall-normal direction. The simulations start with a laminar boundary layer at the inflow which is triggered to transition by a random volume force near the wall. A fringe region is added at the end of the computational domain to enable simulations of spatially developing flows. In this region the flow is forced from the outflow of the physical domain to the inflow. In this way the physical domain and the fringe region together satisfy periodic boundary conditions. Details can be found in Yudhistira & Skote (2011).

The time integration is performed using a third-order Runge-Kutta-scheme for the non-linear terms and a second-order Crank-Nicolson method for the linear terms. A 3/2-rule is applied to remove aliasing errors from the evaluation of the non-linear terms when calculating FFTs in the wall parallel plane.

Numerical parameters

All quantities are non-dimensionalized by the freestream velocity (U) and the displacement thickness (δ^*) at the starting position of the simulation ($x = 0$), where the flow is laminar. The Reynolds number is set by specifying $Re_{\delta^*} = U\delta^*/\nu$ at $x = 0$. In all the simulations presented here, $Re_{\delta^*} = 450$. The computational box is 600 in simulation length units (δ^*) long (including 100 units for the fringe), 30 units high and 34 units wide. The resolution used for the simulations were 1000 modes in streamwise direction, 217 modes in wall-normal direction, and 200 modes in the spanwise direction. This grid size result in a spatial resolution of $\Delta X^+ \times \Delta Z^+ \times \Delta Y^+_{mean} = 13.6 \times 3.9 \times 3.1$, with ΔY^+_{min} close to the wall at 0.036. Note that unless otherwise stated, the $+$ superscript indicates that the quantity is made non-dimensional with the friction velocity of the unmanipulated boundary layer (the reference case) at $x = 250$, denoted u^0_τ, and the kinematic viscosity (ν).

The sampling time for the reference case was 10000 in time units (δ^*/U), started only after a stationary flow (in the statistical sense) was reached. In the case with wall forcing, the total sampling time was 23000 after an initial simulation time of 4000 with oscillations.

As the fringe starts at $x = 500$, only results up to $x = 470$ will be utilized to avoid any upstream influence of the fringe. The transition region is roughly between $x = 5$ (where the trip is located) and $x = 150$. Thus, the region of a fully developed turbulent boundary layer, free from any influence of the numerical method, is $x = 150 - 470$. The Reynolds number based on the momentum thickness (Re_θ) is varying between 390 and 750 in this region for the unmanipulated (reference) boundary layer. In inner scaling (based on the friction velocity at $x = 250$), the region amounts to about 7000 wall units.

The wall oscillation in the form of a travelling wave in the present simulations is applied in the spanwise direction over a particular region in streamwise direction. Therefore, the form of this boundary condition is given by

$$w|_{y=0} = W_m f(x) \sin[\kappa(x - x_{start}) - \omega(t - t_{start})] \qquad (4)$$

where a profile function $f(x)$ is utilized to select the domain where the oscillation takes place, and is given by,

$$f(x) = S\left(\frac{x - x_{start}}{\Delta x_{rise}}\right) - S\left(\frac{x - x_{end}}{\Delta x_{fall}} + 1\right), \qquad (5)$$

with x_{start}, x_{end}, x_{rise} and x_{fall} set to 250, 487, 5 and 5 respectively. $S(x)$ is a continuous step function that rises from zero for negative x to unity for $x \geq 1$. The expression of $S(x)$, which has the advantage of having continuous derivatives of all orders is,

$$S(x) = \begin{cases} 0, & x \leq 0, \\ 1/(1 + e^{(1/(x-1)+1/x)}), & 0 < x < 1, \\ 1, & x \geq 1. \end{cases} \qquad (6)$$

The remaining parameters in equation (4) are given in both outer and inner scalings in table 1. In order to distinguish the time averaged statistical mean from the phase averaged mean, a total of 36 individual statistics was created, i.e. a total of 36 bins were used to resolve one period of the oscillations.

Table 1. Travelling wave parameters.

W_m	W_m^+	κ	λ_x^+	ω	T^+
0.606	12	0.37	384	0.041	176

RESULT

We present both total and phase-wise statistics in the various sections below.

Skin friction

The friction coefficient is defined as

$$C_f = 2\left(\frac{u_\tau}{U_\infty}\right)^2, \qquad (7)$$

where the friction velocity u_τ is calculated from the mean streamwise velocity gradient at the wall:

$$u_\tau \equiv \sqrt{\nu \left.\frac{\partial u}{\partial y}\right|_{y=0}} \qquad (8)$$

In Figure 1 the skin friction coefficient is shown as a function of the streamwise coordinate (x). The reference case is shown as the blue curve while phase $\phi = 0^\circ$

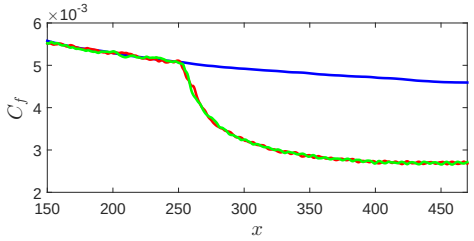

Figure 1. Skin friction for the reference boundary layer (blue), and the controlled boundary layer for phase $\phi = 0^\circ$ (red) and $\phi = 90^\circ$ (green). The wall forcing starts at $x = 250$.

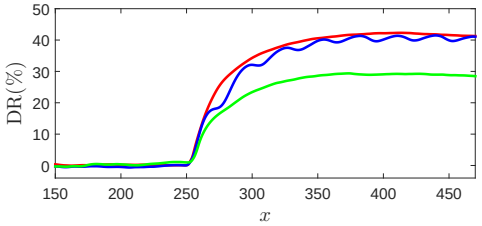

Figure 2. DR for the travelling wave forcing (red); temporal forcing cases with $T^+ = 132$ (green) ; spatial forcing with $\lambda_x^+ = 1320$ (blue).

and $\phi = 90^\circ$ are presented in red and green colors, respectively. The large differences between the phases observed by Lardeau & Leschziner (2013) in the case of pure temporal forcing are not detected here. In addition, only weak fluctuations (which follow the undulating wall velocity, as will be discussed later) are discovered downstream of the spatial transients (at roughly $x = 300$). This is in contrast to the findings of Skote (2011, 2013), where stronger variation was detected for the pure spatial forcing. Note that the spatial oscillations seen in the phase-wise statistics will cancel each other in the total statistics, which is why the DR profile in figure 2 is a smooth curve.

The drag reduction (DR) is calculated from

$$\mathrm{DR}(\%) = 100\frac{C_f^0 - C_f}{C_f^0}, \tag{9}$$

where C_f^0 is the skin friction of the unmanipulated boundary layer (reference case). In addition, previous simulations (Skote, 2013) with a pure temporal forcing (equation 1) and a pure spatial forcing (equation 2) is shown for comparison. Both of these additional cases were performed with the same amplitude ($W_m^+ = 12$) as in the present simulation. Note that the pure spatial forcing produce a spatially fluctuating DR. On the other hand, the present travelling wave forcing yields a smooth profile of the DR since the spatial variation is averaged out when performing the temporal averaging.

The DR reached with the travelling wave as forcing is around 42%, slightly less than what was obtained (45%) in channel flow by Quadrio *et al.* (2009). The Reynolds number in their case was $Re_\tau = 200$ which translates to $Re_\Theta = 464$, as compared to $Re_\Theta = 500 - 730$ in the present

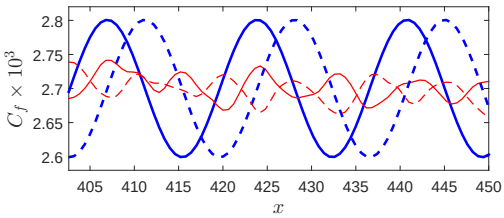

Figure 3. Skin friction coefficient (red) together with the (scaled) wall velocity (blue) at two different phases. (Solid lines) $\phi = 0^\circ$; (broken lines) $\phi = 90^\circ$.

simulation. In addition, the simulations with pure temporal wall oscillations also resulted in DR values for the boundary layer slightly lower than the corresponding ones from the channel flow (Skote, 2012). Note that lower DR values is consistent with the rapid decay of DR for increasing Re at low values of Re. In order to convert the Reynolds numbers, the expression proposed by Schlatter & Örlü (2010)

$$Re_\tau = 1.13 \times Re_\Theta^{0.843} \tag{10}$$

is used.

Finally, we make the remark that from a total energy saving point of view, i.e. if the energy spent on the oscillations are accounted for in the overall energy budget, the present simulations with high amplitude ($W_m^+ = 12$) of the forcing cannot generate a positive result.

When considering only one of the 36 separate set of statistics (i.e. considering approximately a single phase in time of the forcing), the wall velocity remains constant in time but is varying sinusoidal in space. An example of the wall velocity is given in figure 3. Included is also the corresponding skin friction profiles. The C_f is fluctuating with half the wavelength and the crests and troughs correspond roughly to the maximum/minimum and zero-crossings in the all velocity, respectively. Thus, the same correlation as found in the spatial forcing by Skote (2011) is generated phase-wise by the travelling wave. Note that the different phases do not yield temporally varying DR (with the mean taken spatially), in contrast to the case pure temporal forcing with the long period of $T^+ = 200$ as shown by Lardeau & Leschziner (2013). Note that the less converged C_f profiles are due to that only 1/36 of the total statistics is being used.

To investigate more quantitatively the relation between the wall velocity and C_f all the phases are added together, taking into account the phase shift. The result is shown in figure 4. Here a small phase shift is revealed, similar to the results for the temporal forcing in channel flow presented by Agostini *et al.* (2014). By examining the phase shift in figure 4 carefully, the distance can be quantified to be $\Delta x = 1.2$. Hence, the spatial phase shift is $\Delta x = \lambda_x \times 0.071$. From the plots of the time variation of the skin friction and wall velocity in Agostini *et al.* (2014), one can calculate that the temporal phase shift in their channel flow is $\Delta T = T \times 0.071$, i.e. exactly the same shift in phase between the skin friction and wall velocity is occurs.

In figures 3 and 4 the wall velocity is rescaled to fit the graph according to the formula $W_{wall}/6 + 2.7$.

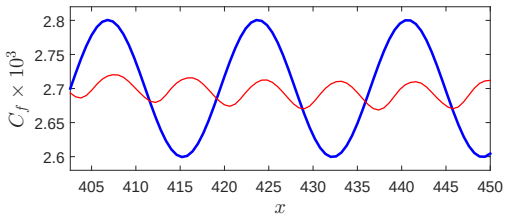

Figure 4. Skin friction coefficient (red) together with the (scaled) wall velocity (blue) with all the phases added together, taking into account the spatial phase shift.

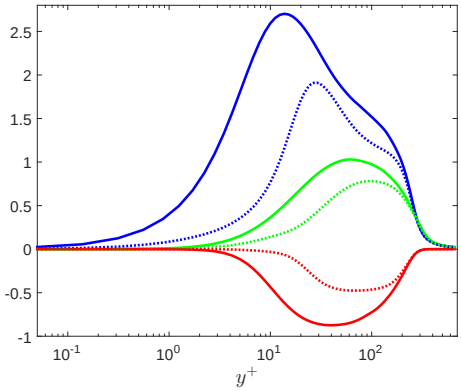

Figure 5. Reynolds stresses at $x = 402$. (blue) u^+_{rms}; (green) v^+_{rms}; (red) $\overline{uv}^+$; the solid curves are the unmanipulated boundary layer; the dotted curves are for the oscillating wall cases, scaled with u^0_τ.

Reynolds stresses

The longitudinal (*rms*-value), normal (*rms*-value), and shear Reynolds stresses respectively scaled with u^0_τ are shown in figure 5 for the position $x = 402$. The choice of u^0_τ as velocity scale provides a comparison in absolute terms with the reference case. The curves actually follow the results provided by Skote (2013) closely, which is consistent with the similar DR result shown in figure 2.

In order to investigate the alternation of the turbulence structure due to the forcing, the profiles scaled with the actual u_τ are presented in figure 6. In this case, we note that only the longitudinal Reynolds stress has a peak value lower for the controlled case compared to the reference case, while the peak of all Reynolds stresses have shifted outward.

The only component varying downstream due to the non-uniform wall forcing is the spanwise component, which therefore is examined separately in the next section.

Spanwise Reynolds stress

In this section, the scaling is based on simulation coordinates in order to remove any ambiguity and facilitate the comparison with earlier simulations and analysis of the spanwise Reynolds stress. A region of the computational box is shown in figure 7. The statistics from only one of the phase-wise statistics is shown ($\phi = 0°$). The spanwise Reynolds stress is illustrated by the colours, where blue is small magnitude and red is high. Of all the turbulence statistics, it is w_{rms} which exhibits the strongest variation spatially.

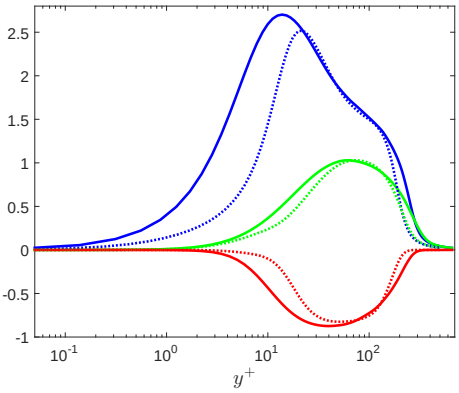

Figure 6. Reynolds stresses at $x = 402$. (blue) u^+_{rms}; (green) v^+_{rms}; (red) $\overline{uv}^+$; the solid curves are the unmanipulated boundary layer; the dotted curves are for the oscillating wall cases, scaled with the actual (local) u_τ.

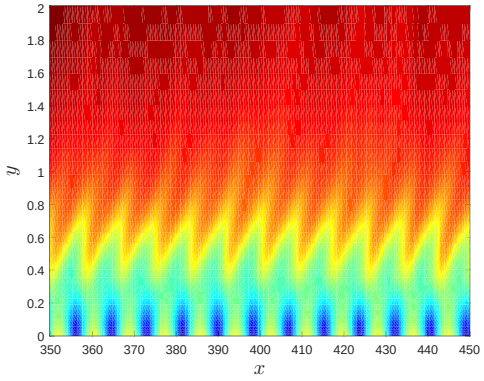

Figure 7. Spanwise Reynolds stress for one of the 36 phases in a section of the computational box close to the wall. Note that the region has been stretched in the wall-normal direction (y).

The spanwise Reynolds stress for eight positions downstream of the $x-$position where the wall velocity (spanwise forcing) is zero is shown in figure 8. The positions are chosen such that the distance between the profiles is one-eighth of a wave-length, i.e. $\lambda_x/8$. Similar to the pure spatial forcing case presented in Skote (2013), the profiles at positions $1/8\ \lambda_x$ and $5/8\ \lambda_x$ coincides, as well as the corresponding profiles at $2/8$, $6/8$ and $3/8$, $7/8$ and $4/8$, $8/8$. The latter profile in each couple is plotted as a broken line, but is indistinguishable from the former profiles. Here, each phase has been evaluated separately and then added together, taking into account the phase-speed of the travelling wave.

A much weaker distinction between the various profiles than what was observed in the simulations by Skote (2013) is detected here. The reason is the much smaller wavelength used in the present simulation. This is consistent with the weaker spatial variation of the skin friction. Furthermore, the peak of the spanwise Reynolds stress does not move closer to the wall in the present simulation, in contrast to the pure spatial forcing case (Skote, 2013), due

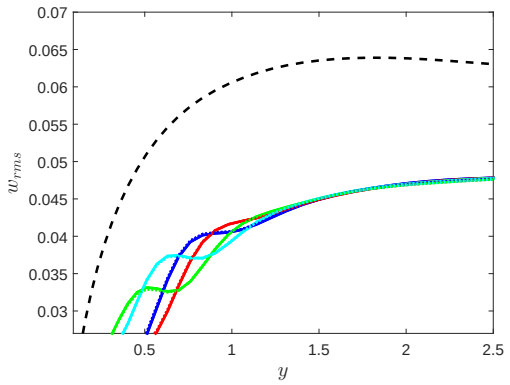

Figure 8. Spanwise Reynolds stress profiles for the 36 phases added together. $x-$positions for the profiles relative to where the wall velocity is zero: (blue solid) $1/8\ \lambda_x$; (red solid) $2/8\ \lambda_x$; (green solid) $3/8\ \lambda_x$; (cyan solid) $4/8\ \lambda_x$; (blue broken) $5/8\ \lambda_x$; (red broken) $6/8\ \lambda_x$; (green broken) $7/8\ \lambda_x$; (cyan broken) $8/8\ \lambda_x$; $(--)$ reference case.

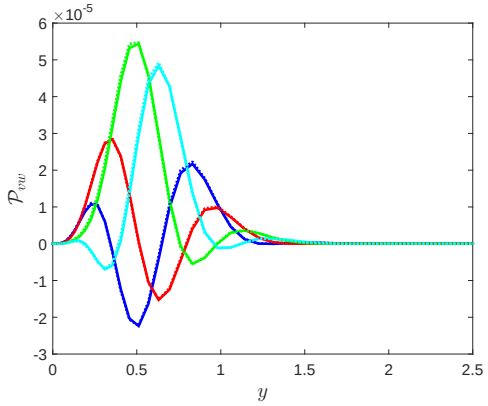

Figure 9. $\mathscr{P}_{vw}$ profiles for the 36 phases added together. $x-$positions for the profiles relative to where the wall velocity is zero: (blue solid) $1/8\ \lambda_x$; (red solid) $2/8\ \lambda_x$; (green solid) $3/8\ \lambda_x$; (cyan solid) $4/8\ \lambda_x$; (blue broken) $5/8\ \lambda_x$; (red broken) $6/8\ \lambda_x$; (green broken) $7/8\ \lambda_x$; (cyan broken) $8/8\ \lambda_x$.

to the lack of the violent phase variation seen with that kind of forcing.

Spanwise Reynolds stress production

When seeking an explanation for the variation in the spanwise Reynolds stress, it is natural to look at the production term in the transport equation for this component:

$$\mathscr{P}_{33} = \mathscr{P}_{vw} + \mathscr{P}_{uw} = -2\overline{v'w'}\frac{\partial w}{\partial y} - 2\overline{u'w'}\frac{\partial w}{\partial x} \qquad (11)$$

Both $\mathscr{P}_{vw}$ and $\mathscr{P}_{uw}$ are zero for the unforced boundary layer, while the latter is zero in the pure temporal forcing case. In contrast, both terms are non-zero for the spatial or travelling wave forcing. The two production terms in equation (11) are directly related to the wall oscillation since $\partial w/\partial y$ and $\partial w/\partial x$ are involved in $\mathscr{P}_{vw}$ and $\mathscr{P}_{uw}$, respectively. The streamwise derivative $(\partial w/\partial x)$ is non-zero only for the spatially varying forcing.

To extract the production term $\mathscr{P}_{33}$ in a temporal case (including travelling wave) is a non-trivial task. The decomposition of the flow needs to be refined, and can be written as: $\widetilde{u}_i = \langle u_i \rangle + u_i''$, where $\langle u_i \rangle$ is the phase averaged $\widetilde{u}_i$ and u_i'' is the stochastic fluctuations, separated from the phase fluctuations. u_i'' relates to the total fluctuations u_i' through $u_i'' = u_i' - (\langle u_i \rangle - u_i)$. Hence, u_i'' is the total fluctuations with the periodic fluctuations removed. With this formulation, the production becomes:

$$\mathscr{P}_{33} = \mathscr{P}_{vw} + \mathscr{P}_{uw} = -2\overline{\langle v''w'' \rangle \frac{\partial \langle w \rangle}{\partial y}} - 2\overline{\langle u''w'' \rangle \frac{\partial \langle w \rangle}{\partial x}} \qquad (12)$$

The two production terms are presented in figures 9 and 10, respectively. Here, the phase averaging has been performed, and then the result for the various phases has been summed up, taking into account the phase-shift in order to get the profiles for the different positions relative to the phase in space. Clearly, $\mathscr{P}_{vw}$ is the dominant term, while $\mathscr{P}_{uw}$ has more negative contribution. Both therms are

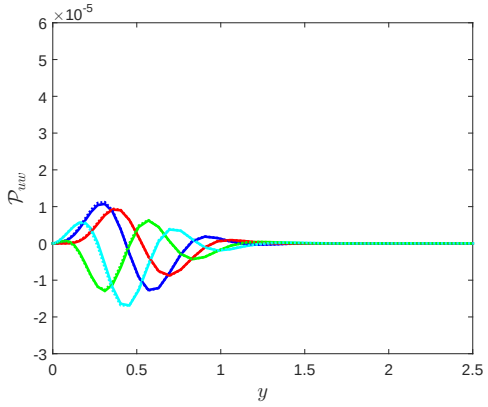

Figure 10. $\mathscr{P}_{uw}$ profiles for the 36 phases added together. Legend as for figure 9.

exactly periodic with half the forcing wavelength as the profiles separated by one half-wavelength collapse (solid and broken lines). The summation over all the spatial location over one wavelength is presented in figure 11, and indeed the contribution from $\mathscr{P}_{uw}$ is negative except for a small region close to the wall. This inner positive peak is a unique feature which was not observed in the case of pure spatial forcing (Skote, 2013).

CONCLUSION

For the first time are results from a forcing in the form of a travelling wave of the turbulent boundary layer presented.

No variation of the skin friction (apart from those originating due to the travelling wave forcing) for the different phases is detected in contrast to the pure temporal forcing.

Of the Reynolds stresses, only the spanwise component exhibits strong spatial variation.

The weaker (compared to pure spatial oscillations) streamwise variation of the skin friction and spanwise Reynolds stress are due to the shorter wavelength of the

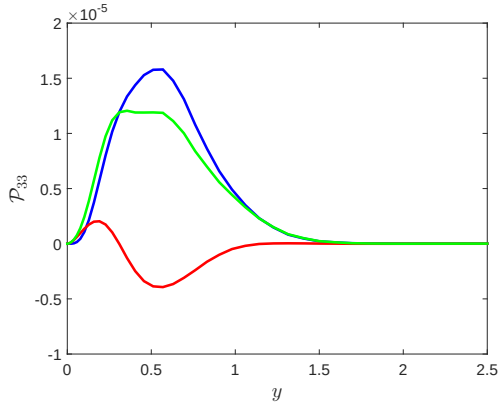

Figure 11. Profiles for the 36 phases added together and summed over all $x-$positions covering one wavelength. (blue) $\mathscr{P}_{vw}$; (red) $\mathscr{P}_{uw}$; (green) $\mathscr{P}_{33}$.

present travelling wave forcing.

The spatial phase shift between wall velocity and skin friction is similar to the temporal phase shift in channel flow with pure temporal wall forcing.

By separating phase and stochastic fluctuations, the production of spanwise Reynolds stress can be investigated. Two distinct contributions are identified, and their positive and negative values over one wavelength in space are presented.

REFERENCES

Agostini, L., Touber, E. & Leschziner, M. A. 2014 Spanwise oscillatory wall motion in channel flow: drag-reduction mechanisms inferred from DNS-predicted phase-wise property variations at Re = 1000. *J. Fluid Mech.* **743**, 606–635.

Auteri, F., Baron, A., Belan, M., Campanardi, G. & Quadrio, M. 2010 Experimental assessment of drag reduction by traveling waves in a turbulent pipe flow. *Phys. Fluids* **22 (115103)** (11).

Chevalier, M., Schlatter, P., Lundbladh, A. & Henningson, D. S. 2007 Simson — a pseudo-spectral solver for incompressible boundary layer flows. Technical report. TRITA-MEK 2007:07, KTH Mechanics, Stockholm, Sweden.

Choi, K.-S. 2002 Near-wall structure of turbulent boundary layer with spanwise-wall oscillation. *Phys. Fluids* **14**, 2530–2542.

Choi, K. S. & Clayton, Brian R. 2001 The mechanism of turbulent drag reduction with wall oscillation. *Intl J. Heat Fluid Flow* **22** (1), 1–9.

Di Cicca, G. M., Iuso, G., Spazzini, P. G. & Onorato, M. 2002 Particle image velocimetry investigation of a turbulent boundary layer manipulated by spanwise wall oscillations. *J. Fluid Mech.* **467**, 41–56.

Ibrahim, I.H. & Skote, M. 2012 Simulations of the linear plasma synthetic jet actuator utilizing a modified Suzen-Huang model. *Phys. Fluids* **24 (113602)** (11).

Jung, W. J., Mangiavacchi, N. & Akhavan, R. 1992 Suppression of turbulence in wall-bounded flows by high-frequency spanwise oscillations. *Phys. Fluids A* **4** (8), 1605–1607.

Laadhari, F., Skandaji, L. & Morel, R. 1994 Turbulence reduction in a boundary layer by a local spanwise oscillating surface. *Phys. Fluids* **6**, 3218–3220.

Lardeau, S. & Leschziner, M. A. 2013 The streamwise drag-reduction response of a boundary layer subjected to a sudden imposition of transverse oscillatory wall motion. *Phys. Fluids* **25** (7).

Negi, P. S., Mishra, M. & Skote, M. 2015 DNS of a single low-speed streak subject to spanwise wall oscillations. *Flow Turbul. Combust.* **94** (4), 795–816.

Quadrio, M. & Ricco, P. 2011 The laminar generalized Stokes layer and turbulent drag reduction. *J. Fluid Mech.* **667**, 135–157.

Quadrio, M., Ricco, P. & Viotti, C. 2009 Streamwise-travelling waves of spanwise wall velocity for turbulent drag reduction. *J. Fluid Mech.* **627**, 161–178.

Ricco, P. 2004 Modification of near-wall turbulence due to spanwise wall oscillations. *J. Turbul.* **5**, 24.

Ricco, P. & Wu, S. 2004 On the effects of lateral wall oscillations on a turbulent boundary layer. *Exp. Therm. Fluid Sci.* **29**, 41–52.

Schlatter, P. & Örlü, R. 2010 Assessment of direct numerical simulation data of turbulent boundary layers. *J. Fluid Mech.* **659**, 116–126.

Schlatter, P., Örlü, R., Li, Q., Brethouwer, G., Fransson, J. H. M., Johansson, A. V., Alfredsson, P. H. & Henningson, D. S. 2009 Turbulent boundary layers up to Re-theta=2500 studied through simulation and experiment. *Phys. Fluids* **21 (051702)** (5).

Skandaji, L. 1997 Étude de la structure dune couche limite turbulente soumise à des oscillations trasversales de la paroi. PhD thesis, École Centrale de Lyon.

Skote, M. 2011 Turbulent boundary layer flow subject to streamwise oscillation of spanwise wall-velocity. *Phys. Fluids* **23 (081703)** (8).

Skote, M. 2012 Temporal and spatial transients in turbulent boundary layer flow over an oscillating wall. *Intl J. Heat Fluid Flow* **38**, 1–12.

Skote, M. 2013 Comparison between spatial and temporal wall oscillations in turbulent boundary layer flows. *J. Fluid Mech.* **730**, 273–294.

Skote, M. 2014 Scaling of the velocity profile in strongly drag reduced turbulent flows over an oscillating wall. *Intl J. Heat Fluid Flow* **50**, 352–358.

Trujillo, S. M., Bogard, D. G. & Ball, K. S. 1997 Turbulent boundary layer drag reduction using an oscillating wall. In *AIAA Paper 97-1870*, pp. 1–10. 4th AIAA Shear Flow Control Conf.

Viotti, C., Quadrio, M. & Luchini, P. 2009 Streamwise oscillation of spanwise velocity at the wall of a channel for turbulent drag reduction. *Phys. Fluids* **21 (115109)** (11).

Yudhistira, I. & Skote, M. 2011 Direct numerical simulation of a turbulent boundary layer over an oscillating wall. *J. Turbul.* **12**, N9.